Combined influence of Coulomb interaction and polarons on the carrier dynamics in InGaAs quantum dots

A. Steinhoff,[1] H. Kurtze,[2] P. Gartner,[1,3] M. Florian,[1] D. Reuter,[4] A. D. Wieck,[4] M. Bayer,[2] and F. Jahnke[1]

[1]*Institut für Theoretische Physik, Universität Bremen, 28334 Bremen, Germany*

[2]*Experimentelle Physik 2, Technische Universität Dortmund, 44221 Dortmund, Germany*

[3]*National Institute of Materials Physics, Bucharest-Magurele, Romania*

[4]*Angewandte Festkörperphysik, Ruhr-Universität Bochum, 44780 Bochum, Germany*

(Received 15 July 2013; published 22 November 2013)

Experimental results for the carrier capture and relaxation dynamics in self-organized semiconductor quantum dots are analyzed using a microscopic theory. Time-resolved differential transmission changes of the quantum-dot transitions after ultrafast optical excitation of the barrier states are studied in a wide range of carrier temperatures and excitation densities. The measurements can be explained by quantum-dot polaron scattering and their excitation-dependent renormalization due to additional Coulomb scattering processes. Results of configuration-picture and single-particle-picture descriptions, both with nonperturbative transition rates, show good agreement with the experiments while Boltzmann scattering rates lead to a different excitation density and temperature dependence.

DOI: 10.1103/PhysRevB.88.205309 PACS number(s): 78.67.Hc, 73.21.La, 73.20.Mf, 78.47.jg

I. INTRODUCTION

In the past, extensive investigations of the carrier scattering processes in semiconductor quantum dots (QDs) have been performed both experimentally[1–7] and theoretically[8–18] due to their numerous applications in optoelectronics devices and for semiconductor quantum optics. In QDs the energy levels are completely quantized. From the viewpoint of perturbation theory, energy relaxation of QD-confined carriers toward lower states only occurs when a scattering mechanism exactly fulfills energy conservation in terms of free-carrier states, which is expressed by a δ function in Fermi's golden rule. In the case of phonon scattering, phonon dispersions must be evaluated or multiphonon processes have to be taken into account. However, the longitudinal optical (LO) phonon dispersion is small, and longitudinal acoustic (LA) phonons as well as higher-order processes (such as LO-LA phonon combinations) turned out to contribute only weakly to the redistribution of carriers.[9,15] In experiment, though, efficient carrier relaxation was observed. This has led to the puzzling question of which mechanisms override the "phonon bottleneck". Carrier-carrier interaction processes were proposed,[2] and indeed, when scattering partners are available, Coulomb scattering can provide efficient carrier relaxation. Regarding the interaction with LO phonons, it was demonstrated that perturbation theory does not provide the full answer for modeling QDs and that quasiparticles ("polarons") emerging from the nonperturbative carrier-phonon interaction should be considered.[12,19,20]

Instead of sharp energies, these quasiparticles represent an extended energy range due to phonon replicas and their broadening. Spectral functions reflect these properties, and transition rates depend on the overlap between the spectral functions of the involved states.[21,22] For the low-temperature regime and in the long-time limit, polaron satellites and hybridizations show small broadenings which end up in low scattering rates within a model that solely considers carrier scattering due to polarons. In the ultrafast time domain, however, spectral functions are not yet sharply defined and non-Markovian effects temporally lift the energy-conservation condition.[23,24] It has also been shown that coupling of LO phonons to plasmons in doped heterostructures leads to the formation of quasiparticles referred to as "plasmon LO phonons", which exhibit a stronger dispersion than LO phonons alone and hence enable efficient scattering of QD carriers.[25,26]

Carrier-carrier Coulomb interaction provides additional scattering channels due to the coupling of localized QD states and delocalized states, which are provided by energetically nearby wetting layer (WL) or barrier material. In the past, carrier-carrier Coulomb scattering has been mainly addressed in terms of Boltzmann transition rates.[8,13–16,18,27,28] Such a treatment relies on a single-particle description of carrier excitations. In its simplest form, it is derived from Fermi's golden rule. Quantum kinetic models, e.g., based on the nonequilibrium Green's function technique, allow for the inclusion of non-Markovian effects and quasiparticle renormalizations, e.g., when the carrier scattering is used to determine interaction-induced dephasing in optical absorption and gain spectra.[29,30] Recently it has been pointed out that the co-action of carrier-carrier and carrier-phonon interaction contributes in a nontrivial way, since both interactions lead to quasiparticle renormalizations, which in turn act back on the individual scattering efficiencies.[31] Another question, which has been addressed, is about the use of a configuration-picture description of QD excitations, which accounts for the different multiexciton states, in comparison to the usual single-particle picture description, which considers the averaged carrier populations of the single-particle states.[32]

Among the many issues is the relative importance of carrier scattering with LO phonons versus the Coulomb scattering and their temperature and excitation density dependence. In this paper, we compare systematic experimental results to a novel theoretical approach, which includes the configuration-picture description of QD excitations and the co-action of Coulomb and polaron scattering within a nonperturbative theory.

II. EXPERIMENTAL SETUP AND RESULTS

A. Overview

Time-resolved differential transmission (TRDT) experiments were performed with samples containing ten layers of nominally undoped (In,Ga)As/GaAs QDs. The density of dots in each layer was estimated to 1×10^{10} cm^{-2}. By postgrowth thermal annealing at various temperatures, the confinement potential heights of the QDs (taken as the energy difference between WL and ground-state emission) were shifted in a wide range for different pieces of the as-grown sample. The QD samples were kept in an optical cryostat with a variable temperature insert.

The temporal evolution of carriers in the QDs after pulsed excitation was studied by time-resolved pump-probe spectroscopy: We used two synchronized Ti:sapphire lasers whose emission wavelengths could be tuned independently. Each laser emitted 1.5-ps pulses with a repetition rate of 75.6 MHz and the temporal jitter between the two linearly polarized pulse trains was less than 1 ps. The temporal delay Δt between the pulses was altered with a mechanical delay line with a precision of 100 fs. One laser with variable power served as a pump that excited carriers in the GaAs barrier at 1.55 eV. The other laser, the probe, tested the populations in the QD states. The reference pump excitation density was $I_0 = 40$ W/cm^2; the fixed probe density was ten times weaker. The probe laser energy was tuned over a wide range, mapping all QD-confined states including the WL. From comparison of QD photoluminescence (PL) spectra taken at varying pump excitation power (not shown), we estimate that the average bright exciton occupation per QD is clearly below $\sim$2 per excitation cycle with the reference density I_0.

A pair of balanced photodiodes connected to a lock-in amplifier was employed for detection. The resulting time-resolved transmission signal gives the difference between the probe beam sent through the sample, recorded with or without pump illumination. Thereby the probe absorption under the specific conditions initiated by the initial pump excitation and the subsequent carrier dynamics is detected. The signal is positive if the transmission is enhanced by the pump action, whereas it is negative for pump-reduced transmission.

Our previous experiments[6] on the TRDT dynamics of QD resonances after pulsed optical excitation were performed at 10 K only and are now extended to elevated temperatures. Results are summarized in Fig. 1 for a QD sample where the confinement potential height as defined above is 90 meV. The contour plots show the TRDT versus probe energy and pump-probe delay. The signal as a function of energy provides a mapping of the interband transitions involving the QDs and the WL. The QD shell structure is reflected by the approximately equidistant variation of the transmission amplitude in the energy range from 1.36 to 1.46 eV at 10 K. Three features corresponding to transitions between well-confined electron and hole states are seen, with hints for a fourth confined shell around 1.44 eV which is, however, very close to the WL. This shell and the WL become more apparent in the 80-K transmission plot, where two well-separated features are observed around 1.45 eV. Signals corresponding to negative differential transmission (DT) values arise from exciton states that can be excited only in the presence of carriers excited

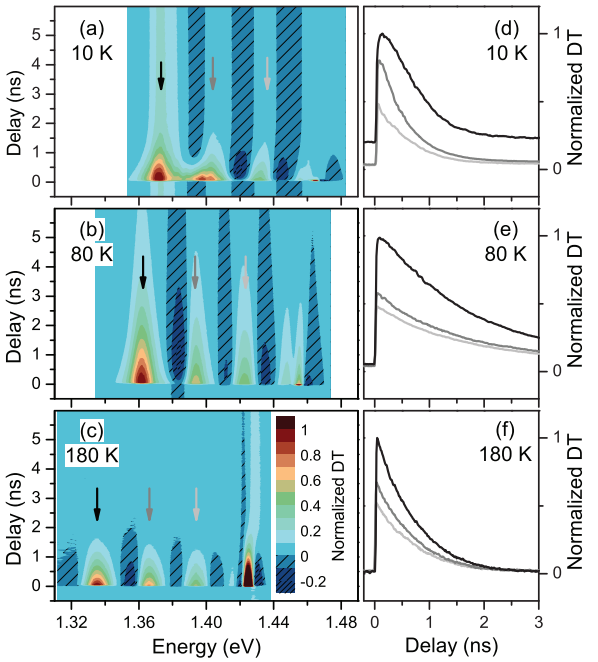

FIG. 1. (Color online) (a)–(c) Contour plot of the differential transmission vs probe energy and pump-probe delay for $T = 10$, 80, and 180 K, recorded on the QD sample with 90-meV confinement potential height. Pump excitation density is I_0 with excitation into the GaAs barrier. (d)–(f) DT traces at the energies marked by the arrows in the left-hand panels, corresponding to the different QD shells.

by the pump pulse. They appear at renormalized energies as compared to the features for the unexcited-dot case due to the influence of Coulomb interactions.

With increasing temperature the transmission features shift in parallel to lower energies due to the band-gap reduction.[33] Concurrently, considerable changes are observed in the temporal evolutions of the TRDT peaks. Two distinct time regimes can be distinguished: The signals rise fast on a few-tens-ps time scale indicating a fast buildup of shell populations, whereas the subsequent decays are much slower. During the short-time range the carrier capture and relaxation dynamics take place, which are the focus of the present paper. For completeness, however, we also discuss the long-time behavior briefly in the next section.

B. Long-time behavior

Variation of the temperature affects the different transmission traces corresponding to the QD shells in a similar manner at long delays. In general, the behavior in this range is largely determined by the radiative recombination of bright exciton complexes. At 10 K the TRDT signals can be approximated by biexponential decays with a fast and a much slower component, as seen from Figs. 1(d) and 1(c), showing transmission traces as function of delay for the three energies corresponding to the TRDT maxima of the confined QD shells. From time-resolved photoluminescence we know that the radiative ground-state exciton lifetime in the studied sample with 90 meV confinement potential is 0.4 ns.[34,35] This time corresponds well to the decay time of the fast component of the ground-state differential transmission, so we relate it

to recombination of bright excitons. For the excited shells, the fast decays occur on comparable time scales with a slight acceleration in particular for the first excited shell, most likely due to relaxation into lower-lying shells in addition to the radiative decay.

The long-lived signal is particularly pronounced for the ground state and can be assigned to dark exciton population.[6,36] The exchange interaction splitting between dark and bright excitons is on the order of 0.1 meV, leading to an exciton spin relaxation between these two reservoirs that is slow compared to the bright exciton radiative decay. The slow signals for the excited states are contributed by an incomplete relaxation of carriers. The decay times of both contributions exceed the pump-pulse separation, giving rise to the TRDT signals at negative delays reflecting the aftermath of the pump pulse preceding the pulse at time zero by 13.2 ns.

With increasing temperature up to 80 K, the populations surviving the pump-pulse separation disappear in all shells. However, also the fast decaying component is slowed down, so that the two-component behavior is smeared out indicating coupling between the bright and dark exciton reservoirs. We attribute this behavior to thermal activation of exciton spin relaxation. At 80 K the spin-relaxation time apparently is in the nanosecond range, comparable to the bright exciton radiative decay, so that the bright exciton reservoir becomes efficiently fed through dark exciton spin relaxation. As a result the fast-decaying component of the ground state is decelerated. In addition, also the corresponding TRDT decays of the excited-shell signals become slower due to thermal population.

Further increase of the temperature up to $T = 180$ K leads to a shortening of decays, so that basically only the fast component is present, independent of the considered shell: The TRDT amplitude evolutions of the three shells are almost identical so a thermal exchange of carriers between the confined states occurs. The third excited shell, quasiresonant with the wetting layer, becomes depopulated particularly fast. At 180 K thermal activation also leads to a long-lasting carrier population in the WL, while at lower temperatures this population is rather short lived, shorter than the QD populations, indicating efficient carrier capture into the quantum dots. By contrast, at 180 K traces of the wetting layer population can be seen even at negative delays, so that carriers survive there over times exceeding the pulse repetition period. From following the transmission trace with time, also the influence of Coulomb interactions and the resulting renormalization of transition energies can be assessed, as discussed already above for the negative DT values. As long as appreciable carrier populations are present in the QD shells, the WL-related transmission feature is shifted to lower energies compared to the times after decay of the dot populations when the line appears at energies about 5 meV higher.

C. Short-time behavior

Let us turn now to the early time evolutions of the TRDT signals, during which the pump excitation populations build up due to carrier capture and relaxation. The inset in Fig. 2 contains examples of TRDT traces for the three studied temperatures at fixed excitation power $I_0/3$. To assess the underlying dynamics more quantitatively, we have

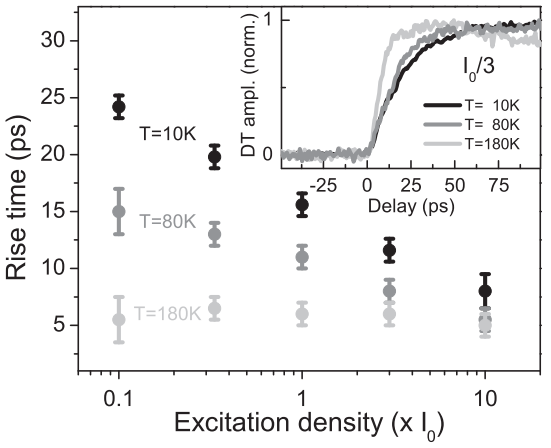

FIG. 2. Rise times extracted from TRDT transients of the QD ground state, obtained at various excitation intensities for temperatures $T = 10$, 80, and 180 K. The inset shows DT traces at an excitation density of $I_0/3$. In the figure and inset, QD confinement potential height is 90 meV, with excitation into GaAs at 1.55 eV photon energy.

analyzed the DT signal increase by monoexponential fits. The dependence of the rise times of the ground-state transition signal determined thereby is shown in Fig. 2 versus excitation intensity at temperatures $T = 10$, 80, and 180 K. The data for $T = 10$ K underline the importance of carrier-carrier scattering processes for relaxation, as seen from the strong drop of the rise time with excitation density. In contrast, the rise times at $T = 80$ K show a weaker variation with excitation density and at $T = 180$ K almost no dependence remains. These results indicate a relaxation pathway which opens up and becomes efficient with increasing temperature. This behavior is analyzed in more detail below in Sec. IV.

Another important parameter is the energy spacing of the confined electron and hole QD levels, $\Delta E_{e,h}$. When applying perturbation theory, the LO-phonon scattering efficiency should strongly depend on $\Delta E_{e,h}$, becoming significant only for the resonance case. However, in the nonperturbative treatment based on the polaron picture, fast relaxation is not limited to a strict resonance condition. As demonstrated in Ref. 21 the spectral functions of a coupled carrier-phonon system can lead to fast relaxation on a picosecond scale even for considerable detuning of $\Delta E_{e,h}$ with respect to the LO-phonon energy. Additional Coulomb scattering processes, which exhibit a pronounced increase in efficiency with the excitation density, further reduce the dependence of the scattering processes on $\Delta E_{e,h}$.

These findings are confirmed in our experiments. As a measure for the confined level splitting we use two quantities which are directly experimentally accessible. Besides the already mentioned confinement potential height, this is the approximately equidistant energy splitting between the emission bands from different QD shells in high-excitation photoluminescence. This splitting is determined by the sum of the electron and hole confined level splittings modified by Coulomb interaction effects. Both quantities are linked to each other.

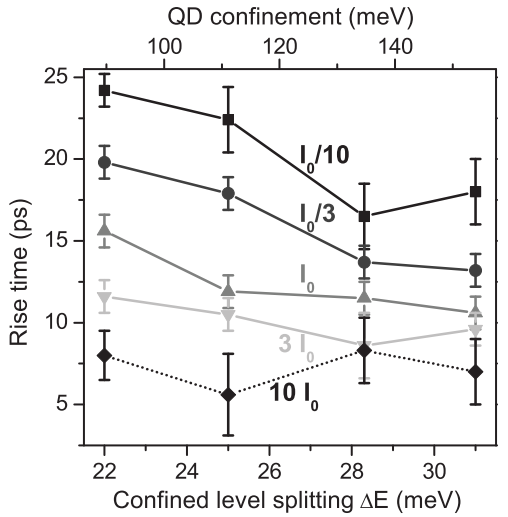

FIG. 3. Rise times of the TRDT ground-state signal vs QD shell splitting obtained from high-excitation PL. The shell splitting (bottom axis) is intimately related to the confinement potential height given at the top axis. The data sets correspond to different excitation intensities in units of the reference density I_0. All data points indicate excitation into GaAs at 1.55 eV photon energy.

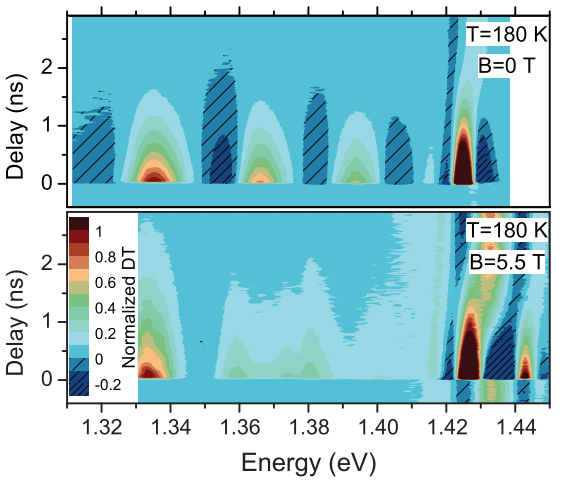

FIG. 4. (Color online) Contour plots of the differential transmission vs probe energy and pump-probe delay for $B = 0$ (top) and $B = 5.5$ T (bottom) at $T = 180$ K. Pump density is I_0 with excitation into the GaAs barrier at 1.55 eV photon energy. In both cases, the QD sample with 90 meV confinement potential height was used.

Different values for these two quantities are accessible through the series of samples annealed at different temperatures. Figure 3 shows TRDT rise times of the ground-state transmission versus different shell splittings (bottom axis) and confinement potential heights (top axis), respectively, recorded for different excitation powers. For all confinement potentials the rise time considerably decreases with increasing excitation density, which reflects the influence of Coulomb-mediated scattering processes. Irrespective of this dependence, even for the lowest excitation power a rapid buildup of the ground-state population is observed for the different shell splittings studied with a resonant shortening for a splitting around 28 meV.

The apparent weak dependence of the population rise times on the energy splitting between the QD shells can be highlighted also by another experiment. As mentioned, the confined level structure of the QDs is reflected by the equidistant TRDT features in Fig. 1. Application of a longitudinal magnetic field leads to a splitting of the shells that can be well described by the Fock-Darwin spectrum,[37] even when including many-body effects. As a result the level structure becomes anharmonic with widely varying splittings between confined shells. Corresponding experiments for the TRDT are shown in Fig. 4, recorded at a field strength of 5.5 T as compared to the zero-field case. The temperature was 180 K. The changes of the level structure by the magnetic field are apparent from this contour plot. Still the rise times of the different transmission features remain short as a result of efficient carrier relaxation, even though the shell splittings deviate considerably from the LO-phonon energy. The ground-state population becomes even more dominant compared to the higher-lying shell populations. The negative TRDT features disappear when the field is applied. Note also that for the wetting layer two well-separated transmission features show up in the magnetic field which reflect Landau-level formation, for which again pronounced shifts with time are observed due to changes of Coulomb interaction with varying dot carrier density.

III. THEORETICAL ANALYSIS

The temperature and excitation density dependence of the experimental results for the rise time of the differential transmission in Fig. 2 point to an interplay between carrier-phonon and WL-assisted carrier-carrier relaxation processes.

To elucidate the role of different mechanisms, we evaluate the QD carrier dynamics using two fundamentally different approaches. Within a single-particle description the excitation of the QD states is determined by one-particle occupation probabilities f_i, which are calculated from kinetic equations. Alternatively, we use a configuration-picture description, in which the QD carriers are represented by a density operator $\rho(t)$ in a many-particle configuration basis. The dynamical evolution of $\rho(t)$ follows from a direct solution of the von Neumann equation. As we discussed in Ref. 32, this description accounts for Pauli and Coulomb correlations between the few QD carriers, induced by the exclusion principle as well as the Coulomb interaction between the QD carriers, respectively.

These two approaches are further defined by the way the interaction processes enter the evaluation of the scattering rates. In both cases, carrier scattering processes are introduced by the coupling of QD carriers to (i) a bosonic bath of LO phonons and (ii) a fermionic bath of WL carriers. For this purpose, we use a nonperturbative description of carrier scattering processes, in which the central role is played by the renormalized spectral functions. They include the joint contributions of carrier-carrier and carrier-phonon interaction to determine renormalized quasiparticle properties for the QD carriers. The same spectral functions are then used for the calculation of the carrier-phonon as well as the carrier-carrier scattering rates. These rates enter both the von Neumann equation via the Lindblad terms, and the kinetic equations via single-particle scattering rates. Therefore, in what concerns

the transition rates, the two approaches are treated on equal footing.

Additionally, for a direct comparison, in Sec. IV below we also present results for the single-particle kinetic equations using perturbative Boltzmann scattering integrals, as provided by Fermi's golden rule. In this case, the transition rates do not include quasiparticle renormalizations and strict energy conservation appears in terms of free-carrier energies. Then the carrier-phonon and carrier-carrier scattering rates become independent of each other and the population factors determine only the availability of initial and final states.

A. Description of QD-carrier dynamics

The bound states in each QD consist of ground and excited states in each band. These are the single-particle states provided by the QD confinement potential. In the first approach, a single-particle basis $|i\rangle$ is used for the QD and the WL states and the excitation dynamics is described in terms of single-particle occupation probabilities f_i. If we restrict ourselves to Markovian dynamics, the equation of motion for f_i can be written as

$$\frac{\partial f_i}{\partial t} = (1 - f_i)S_i^{\text{in}} - f_i S_i^{\text{out}}, \tag{1}$$

with the rates S_i^{in} and S_i^{out} describing in- and out-scattering for the single-particle states, respectively. Considering the quasicontinuous density of states of the environment, the latter acts as an energy and particle reservoir for the QDs. In general, the dynamics of phonons and WL carriers follows their own kinetic equations. However, this is beyond the scope of this paper and not necessary for the presented experiments. As a result of ultrafast thermalization processes, it is assumed that phonons and WL carriers are in thermal equilibrium with given temperature and WL-carrier density. Then scattering rates have to be calculated only for i being a QD state index.

In the past it has been pointed out that in QD systems, due to the finite state space of the electronic excitations and the strong Coulomb configuration interaction, carrier correlations are of increasing importance and a configuration-picture description should be more appropriate.[38] Consequences for QD laser threshold current densities[39] or the QD gain recovery dynamics[40] have been discussed. This is the motivation for our second theoretical approach, in which the QD carriers are described by a density operator $\rho(t)$ that is expressed in a configuration basis. This leads to a full many-body description of the QD excitations, in which the Coulomb configuration interaction can be directly included. The multiexciton states are the fundamental entities of this approach and their occupation probabilities and transition amplitudes between these configurations are determined.

Denoting the single-particle creation (annihilation) operators by $a_i^\dagger$ (a_i), a given configuration $|I\rangle$ is defined by specifying which single-particle states are occupied ($n_i^I = \langle I|a_i^\dagger a_i|I\rangle = 1$) or empty ($n_i^I = 0$). This approach contains the full information about the QD system, in contrast to the single-particle description. Considering the QD as an open quantum system and, like in the single-particle approach, the coupling to its environment of LO phonons and WL carriers, one can describe the dynamics of the QD density operator by the von Neumann–Lindblad (vNL) equation

$$\dot\rho = -\frac{i}{\hbar}[H_S,\rho] + \sum_X \frac{\gamma_X}{2}[2s_X\rho s_X^\dagger - s_X^\dagger s_X\rho - \rho s_X^\dagger s_X]. \tag{2}$$

The commutator part on the right-hand side represents the quantum-mechanical evolution of the QD excitations, driven by the system Hamiltonian,

$$H_S = H_0 + H_{\text{Coul}}^{\text{QD}}, \tag{3}$$

which consists of the "free" part with the confinement energies ε_i^0,

$$H_0 = \sum_i \hat n_i\ \varepsilon_i^0, \tag{4}$$

and the Coulomb interaction between the QD carriers,

$$H_{\text{Coul}}^{\text{QD}} = \frac{1}{2}\sum_{ijkl} V_{ijkl}\ a_i^\dagger a_j^\dagger a_k a_l\,. \tag{5}$$

As in Ref. 32, we simplify the picture by using an approximate Coulomb Hamiltonian expressed in terms of the number operators $\hat n_i = a_i^\dagger a_i$,

$$H_{\text{Coul}}^{\text{QD}} \approx H_{\text{Coul}}^{\text{diag}} = \sum_{i,j} D_{ij}\hat n_i \hat n_j, \tag{6}$$

which is diagonal in the configuration basis:

$$H_S|I\rangle \approx \left(H_0 + H_{\text{Coul}}^{\text{diag}}\right)|I\rangle = \varepsilon_I|I\rangle. \tag{7}$$

The interaction parameters D_{ij} contain the Hartree and Fock Coulomb integrals, V_{ijji} and V_{ijij}, respectively. In this picture the mixing of configurations is neglected, but their energies are renormalized as

$$\varepsilon_I = \sum_i \varepsilon_i^0 n_i^I + \sum_{i,j} D_{ij} n_i^I n_j^I. \tag{8}$$

Further details about this approximation are discussed in Ref. 41.

Dissipative Lindblad terms are obtained by accounting for the interaction between system and reservoirs with Hamiltonians of the general form

$$H_{SR} = \sum_X s_X \Gamma_X, \tag{9}$$

with system and reservoir operators, s_X and Γ_X, respectively, and summed over some appropriate set of indices. As shown below, both the interaction with phonons and the Coulomb interaction with WL carriers can be cast into this form.

The operator s_X describes a transition between two eigenstates of the system Hamiltonian H_S and the energy change associated with this transition is $\hbar\omega_X$. The usual treatment of the system-reservoir interaction, based on the Born-Markov approximation,[42] is our starting point which is extended subsequently. The transition rate appearing in the corresponding Lindblad term of the vNL equation is

$$\gamma_X(t) = \frac{2}{\hbar^2}\text{Re}\int_0^t dt'\ e^{-i\omega_X(t-t')}\langle\Gamma_X^\dagger(t)\Gamma_X(t')\rangle_R, \tag{10}$$

with the time dependence in $\Gamma_X(t)$ defined by the reservoir Hamiltonian H_R and the average $\langle\cdots\rangle_R$ taken on the reservoir

state. Assuming a reservoir in thermal equilibrium, the reservoir correlator depends only on the time difference and is typically fast decaying with it. Then the lower limit of the time integral can be extended to minus infinity (completed collision approximation[23]), making the transition rates time independent:

$$\gamma_X = \frac{2}{\hbar^2}\mathrm{Re}\int_0^\infty d\tau\; e^{-i\omega_X\tau}\langle\Gamma_X^\dagger(\tau)\Gamma_X(0)\rangle_R. \tag{11}$$

As seen from Eq. (11), the transition rate picks up from the spectrum of the reservoir correlator $\langle\Gamma_X^\dagger(t)\Gamma_X(t')\rangle_R$ precisely the energy lost or gained in the transition. In this sense the Born-Markov rate obeys the rule of exact energy conservation: The energy change in the system is compensated by the reservoir. Examples are encountered below.

The Born-Markov approximation for the transition rates, used in Eqs. (10) and (11), corresponds to the level of Boltzmann scattering rates. When used in the vNL equation these transitions occur between QD configurations while in the Boltzmann equation transitions between single-particle states are considered. Indeed, if in the vNL equation Coulomb and Pauli correlations between the QD carriers are treated in factorization approximation, the Boltzmann equation in the single-particle picture is recovered, as we have discussed in detail in Ref. 32.

Due to the discrete nature of the QD states, the dispersionless phonon spectrum, and the presence of strong interaction processes, it is necessary to use nonperturbative scattering rates in order to prevent unphysical results. This applies to both the single-particle and the configuration-picture description. Specifically we refer to QD polarons and their modification in the presence of Coulomb scattering.

In the following sections we briefly discuss the two types of system-reservoir coupling, namely carrier scattering by LO phonons (including QD-WL and QD-QD transitions) and carrier-carrier Coulomb scattering (in which among the two initial and two final states one, two, and three WL states can contribute). Note that Coulomb interaction solely between QD states is part of the system Hamiltonian. Subsequently, we introduce an ansatz to include renormalizations in the Lindblad rates beyond perturbation theory and discuss the renormalizations that are used for the numerical results in this paper.

B. QD-WL carrier-carrier scattering

The QD in contact with the WL carriers is subject to various Auger-like processes. Carriers are captured or ejected from the QD and they scatter between localized states due to the Coulomb interaction with WL carriers; the latter provide the necessary energy for the transition processes. A detailed analysis of these processes and the corresponding rates have been given in Ref. 32. Here we summarize the used results.

The WL carrier reservoir Hamiltonian is $H_R = \sum_k \varepsilon_k a_k^\dagger a_k$, with k representing both momentum and band index. The system-reservoir Hamiltonian describes the Coulomb interaction between QD and WL carriers. The Coulomb interaction between the QD carriers themselves, Eq. (5), is part of the system Hamiltonian H_S and all indices involved refer to QD states. The system-reservoir interaction has the same form,

$$H_{SR} = \frac{1}{2}\sum_{ijkl} V_{ijkl}\; a_i^\dagger a_j^\dagger a_k a_l\,, \tag{12}$$

but with the difference that now the summation contains both QD and WL indices. To take a specific example, consider the transition of a QD carrier from $|j\rangle$ to $|i\rangle$ facilitated by a WL carrier scattered from $|k'\rangle$ to $|k\rangle$. This is controlled by the terms

$$\begin{aligned}\sum_{k,k'} V_{ikk'j}\; a_i^\dagger a_k^\dagger a_{k'} a_j + \sum_{k,k'} V_{ikjk'}\; a_i^\dagger a_k^\dagger a_j a_{k'}\\ = a_i^\dagger a_j \sum_{k,k'}[V_{ikk'j} - V_{ikjk'}]\; a_k^\dagger a_{k'},\end{aligned} \tag{13}$$

which contains two QD and two WL operators. Similarly, the WL-assisted capture into or ejection out of the QD would contain one QD and three WL operators.

One would be tempted to identify in Eq. (13) s_X with $a_i^\dagger a_j$ and $\Gamma_X = \sum_{k,k'}[V_{ikk'j} - V_{ikjk'}]\; a_k^\dagger a_{k'}$. However, this is not the case, since the operator $a_i^\dagger a_j$ describes many transitions between QD configurations and the energy change is not the same for all. Therefore, the frequency ω_X in Eq. (10) is different for the various possible configurations involved. This is because the initial and final configuration energies depend also on the "spectator" carriers, which do not take part in the transition. A transition event contained in $a_i^\dagger a_j$ takes place between configurations $|J\rangle = a_j^\dagger|\Phi\rangle$ and $|I\rangle = a_i^\dagger|\Phi\rangle$. Here $|\Phi\rangle$ is a reference state which specifies the spectator carriers and in which, of course, the single-particle states i, j are left empty. The corresponding energies are ε_J and ε_I calculated according to Eq. (8). One has now a given transfer energy $\hbar\omega_{IJ} = \varepsilon_I - \varepsilon_J$ for each transfer operator $|I\rangle\langle J|$ contained in $a_i^\dagger a_j$.

As a consequence one identifies the appropriate system operators in H_{SR} as $s_X = s_{IJ} = |I\rangle\langle J|$ with $\Gamma_{IJ} = \Gamma_X$ given above. The corresponding transition rate obtained from Eq. (10) is then

$$\gamma_{IJ} = \frac{2\pi}{\hbar}\sum_{k,k'}|V_{ikk'j} - V_{ikjk'}|^2(1-f_k)f_{k'}\delta(\hbar\omega_{IJ} + \varepsilon_k - \varepsilon_{k'}) \tag{14}$$

in accordance with Fermi's golden rule. The transition from $|J\rangle$ to $|I\rangle$ in the QD is energetically compensated by the scattering from k' to k in the WL reservoir, described with the occupation probabilities f_k.

C. QD carrier scattering by LO phonons

A second type of reservoir is provided by the phonon system. In polar semiconductors the strongest contribution to carrier scattering processes is due to LO phonons, for which we assume a dispersionless spectrum $\omega_{\boldsymbol{q}} = \omega_{\mathrm{LO}}$. The LO-phonon reservoir Hamiltonian is given by

$$H_R = \sum_{\boldsymbol{q}} \hbar\omega_{\mathrm{LO}} b_{\boldsymbol{q}}^\dagger b_{\boldsymbol{q}} \tag{15}$$

and the interaction between the QD system and the phonon reservoir is described by the Hamiltonian

$$H_{SR} = \sum_{i,j,\boldsymbol{q}} g_{\boldsymbol{q}}^{i,j} a_i^\dagger a_j (b_{\boldsymbol{q}} + b_{-\boldsymbol{q}}^\dagger) \tag{16}$$

with the Fröhlich coupling matrix elements $g_{\boldsymbol{q}}^{i,j}$.[43]

In Eq. (16) we have to distinguish between two cases. First, when both indices i,j refer to QD states, electronic transitions $|j\rangle \to |i\rangle$ inside the QD assisted by the emission or absorption of phonons are described, leading to the intra-QD carrier relaxation. The second case involves a QD and a WL state and corresponds to the carrier capture from or reemission into the WL, again assisted by phonons.

Considering for illustration the first case, we encounter here the same situation as in the previous section, namely that one cannot apply the usual Born-Markov procedure directly to $a_i^\dagger a_j$. Again, the many-body correlation description is retained by treating separately the transitions $|I\rangle\langle J|$ between all possible configurations, which include the movement of a carrier from $|j\rangle$ to $|i\rangle$. With the reservoir operator $\Gamma_{IJ} = \sum_{\boldsymbol{q}} g_{\boldsymbol{q}}^{i,j}(b_{\boldsymbol{q}} + b_{-\boldsymbol{q}}^\dagger)$ one obtains from Eq. (11) the transition rate in the form

$$\begin{aligned}\gamma_{IJ} &= \frac{2}{\hbar^2}\mathrm{Re}\int_0^\infty d\tau\; e^{-\frac{i}{\hbar}(\varepsilon_I-\varepsilon_J)\tau} \\ &\quad\times \sum_{\boldsymbol{q}} \left|g_{\boldsymbol{q}}^{i,j}\right|^2 \{(1+N_{\mathrm{LO}})e^{-i\omega_{\mathrm{LO}}\tau} + N_{\mathrm{LO}} e^{i\omega_{\mathrm{LO}}\tau}\} \\ &= \frac{2\pi}{\hbar^2}\sum_{\boldsymbol{q}} \left|g_{\boldsymbol{q}}^{i,j}\right|^2 \{(1+N_{\mathrm{LO}})\,\delta(\omega_{IJ}+\omega_{\mathrm{LO}}) \\ &\quad + N_{\mathrm{LO}}\,\delta(\omega_{IJ}-\omega_{\mathrm{LO}})\}. \end{aligned} \tag{17}$$

N_{LO} is the phonon population at the given lattice temperature. The first term corresponds to processes with phonon emission, the second to absorption.

In Eq. (17) one encounters a problem that is specific to the LO-phonon-driven carrier kinetics in discrete electronic systems. The strict energy-conserving condition expressed by the δ functions is in general not met. In QDs only coincidentally the phonon frequency is resonant with the transition energy. In early theoretical considerations,[44,45] this observation has led to the prediction of a "phonon bottleneck". However, only in lowest-order perturbation theory (Fermi's golden rule) is the scattering rate vanishing. Equation (17) corresponds to this level due to the applied Born-Markov approximation. Nonperturbative treatments lead to the polaron picture with nonvanishing scattering rates.[12,19–22] For the polar coupling in QDs, one even encounters a strong-coupling situation with efficient scattering rates.[21,22] The quasiparticle renormalization effects of the nonperturbative treatment can be included in a generalized form of Eq. (17) via spectral functions, which are the subject of the following section.

D. Quasiparticle renormalizations

A systematic inclusion of interaction processes of arbitrary order is offered by the quantum kinetic theory,[23,24,46] expressed in terms of Kadanoff-Baym equations. In the following, we present an ansatz to combine the configuration-picture description with quantum-kinetic methods and systematically include quasiparticle renormalizations in the QD-carrier interaction with LO phonons and WL carriers.

The Kadanoff-Baym equations lead to results similar to Eq. (17) and corresponding equations for carrier-carrier scattering, but with the exponentials oscillating with the system energies replaced by more complex retarded Green's functions (GFs),

$$\frac{1}{i\hbar}e^{-\frac{i}{\hbar}\varepsilon_I t} \Longrightarrow G_i^r(t). \tag{18}$$

Here, $|i\rangle$ is the single-particle state which is occupied in the configuration $|I\rangle$, but not in the reference configuration $|\Phi\rangle$; see above. Of course, the same replacement goes for the oscillatory exponential containing ε_J. Note that for certain Coulomb scattering processes this can also be true for two single-particle states, so that a product of two GFs appears in Eq. (18). The above replacement corresponds to a substitution of free particles by quasiparticles with a complex spectral structure, which is due to the interaction processes included in the retarded GF,

$$G_i^r(t) = -\theta(t)\frac{i}{\hbar}\langle\Phi|a_i(t)\,a_i^\dagger + a_i^\dagger\,a_i(t)|\Phi\rangle. \tag{19}$$

To simplify the calculation of the retarded GF, often a definite state $|\Phi\rangle$ is used for the averaging, e.g., the vacuum state corresponding to the unexcited system. In contrast, our ansatz is to perform the replacement in Eq. (18) but calculate the retarded GF by taking the average on the particular reference state $|\Phi\rangle$ of the transition from $|J\rangle = a_j^\dagger|\Phi\rangle$ to $|I\rangle = a_i^\dagger|\Phi\rangle$. Hence, the transition between the single-particle states, that defines the transition $|J\rangle \Longrightarrow |I\rangle$, is assumed to take place in the presence of the actual arrangement of "spectator" carriers and the renormalizations they cause. The ansatz ensures that the states occupied by the spectator carriers are Pauli blocked during the evolution and also that the proper Coulomb renormalization is included. On the other hand, one has to keep in mind that $G_i^r(t)$ depends on the reference state; i.e., for a given QD state $|i\rangle$ one has several such GFs, and in calculating γ_{IJ} the appropriate ones need to be used. For notational simplicity we omit in the following the configuration index of the GFs as being obvious from the context.

The retarded GFs obey the spectral Kadanoff-Baym equation[23,24,46]

$$\left(i\hbar\frac{\partial}{\partial t} - \varepsilon_I\right) G_i^r(t) = \delta(t) + \int_0^t dt' \Sigma_i^r(t-t') G_i^r(t'), \tag{20}$$

with the self-energy

$$\begin{aligned}\Sigma_i^r(t-t') &= \delta(t-t')\left\{\Sigma_i^{\mathrm{HF}}(t)\big|_{\mathrm{Coul}} + \Sigma_i^{\mathrm{H}}(t)\big|_{\mathrm{LO}}\right\} \\ &\quad + \theta(t-t')\{\Sigma_i^{>}(t-t')|_{\mathrm{Coul}} - \Sigma_i^{<}(t-t')|_{\mathrm{Coul}} \\ &\quad + \Sigma_i^{>}(t-t')|_{\mathrm{LO}} - \Sigma_i^{<}(t-t')|_{\mathrm{LO}}\}, \end{aligned} \tag{21}$$

where the instantaneous term describes the Hartree-Fock energy renormalization due to Coulomb interaction between QD and WL carriers as well as the Hartree-like one due to LO phonons. The propagators $\Sigma_i^{>}$ and $\Sigma_i^{<}$ contain the quasiparticle renormalizations introduced by the scattering processes. A central ingredient of our theoretical approach is that we include here self-consistently simultaneous contributions from

both carrier-phonon and carrier-carrier interactions. This leads to the fully renormalized spectral functions discussed earlier, which include polaronic as well as Coulomb effects. With these spectral functions the nonperturbative transition rates are calculated. (Note that only the Coulomb interaction processes involving WL states lead to dissipative carrier scattering.)

The LO-phonon contribution to $\Sigma_i^>$ and $\Sigma_i^<$ is the polaron self-energy in self-consistent random-phase approximation:[23,24]

$$\begin{aligned}\Sigma_i^>(t-t')|_{\mathrm{LO}} &= \sum_j (1-f_j) G_j^r(t-t') D_{i,j}^>(t-t'),\\ \Sigma_i^<(t-t')|_{\mathrm{LO}} &= -\sum_j f_j G_j^r(t-t') D_{i,j}^<(t-t'),\end{aligned} \tag{22}$$

which describes quasiparticle renormalizations of the carriers due to their exchange of phonons with the surrounding crystal. The summation runs over both QD and WL state indices. In the former case $f_j = n_j^\Phi$ is the occupancy in the single-particle state j of the reference state $|\Phi\rangle$. For the WL case we take as f_j the thermal equilibrium values. Also the WL retarded GFs are calculated in the absence of the QD, in accordance with the general assumption that the small system does not influence the bath. The phonon propagators in thermal equilibrium are given by

$$\begin{aligned}D_{i,j}^{\gtrless}(t-t') &= \sum_{\boldsymbol{q}} \left|g_{\boldsymbol{q}}^{i,j}\right|^2 d^{\gtrless}(t-t'),\\ d^{\gtrless}(t-t') &= \{(1+N_{\mathrm{LO}})e^{\mp i\omega_{\mathrm{LO}}(t-t')} + N_{\mathrm{LO}} e^{\pm i\omega_{\mathrm{LO}}(t-t')}\}.\end{aligned} \tag{23}$$

For $\Sigma_i^>|_{\mathrm{Coul}}$ and $\Sigma_i^<|_{\mathrm{Coul}}$ in Eq. (21) we use the second-order Born self-energies.[23,24] In Ref. 31 these have been formulated for the Coulomb interaction between QD and WL carriers using self-consistently renormalized spectral functions. As a result, the Coulomb scattering contributes to damping and thus to collision broadening and changes the polaronic GF in a nontrivial way. This in turn modifies all the transition rates.[31]

Replacing the exponential factors in Eq. (17) yields the following expression for the transition rate:

$$\gamma_{IJ} = 2\mathrm{Re}\int_0^\infty dt\, G_i^r(t) G_j^{r,*}(t) D_{i,j}^>(t). \tag{24}$$

The importance of the quasiparticle renormalization is seen by recasting Eq. (24) in terms of the spectral functions, which are obtained from the Fourier transform of the retarded GFs, $\hat{G}_i(\omega) = -1/\pi\ \mathrm{Im}\ G_i^r(\omega)$,

$$\begin{aligned}\gamma_{IJ} &= \frac{2\pi}{\hbar^2}\sum_{\boldsymbol{q}} \left|g_{\boldsymbol{q}}^{i,j}\right|^2 \int\int d\omega\, d\omega' \hat{G}_i(\omega)\hat{G}_j(\omega')\\ &\quad\times\{(1+N_{\mathrm{LO}})\delta(\omega-\omega'+\omega_{\mathrm{LO}}) + N_{\mathrm{LO}}\delta(\omega-\omega'-\omega_{\mathrm{LO}})\}.\end{aligned} \tag{25}$$

As a result, the carrier scattering rate due to LO-phonon emission or absorption is determined by the overlap of the spectral functions for the initial and final states,

$$\int d\omega\ \hat{G}_i(\omega \mp \omega_{\mathrm{LO}})\ \hat{G}_j(\omega). \tag{26}$$

Finally, we abandon the completed-collision approximation, contained for example in Eqs. (17) and (24), and use time-dependent scattering rates, which further softens the energy-conserving condition at small times.

When considering the interaction with both reservoirs simultaneously, the rate of a given transition is

$$\gamma_{IJ} = \gamma_{IJ}^{\mathrm{Coul}} + \gamma_{IJ}^{\mathrm{LO}}. \tag{27}$$

This does not mean that the total effect of the two reservoirs is additive, since the transition rates themselves contain combined influences due to the above-discussed renormalizations.

In the case of phonon scattering the details of the retarded GFs are essential, since Fermi's golden rule with bare-particle energies—usually the dominant contribution in the evaluation of transition rates—is vanishing. This is not the case for the Coulomb rates $\gamma_{IJ}^{\mathrm{Coul}}$. Nevertheless, to be consistent, we use the same retarded GF (containing carrier-phonon and carrier-carrier influences) to modify the Coulomb rates as we used for the carrier-phonon rates.

E. Examples for spectral functions

The quasiparticle GFs show a rich spectrum of Fourier components, instead of the single frequency of the bare particle. This makes the difference between Eq. (17), which predicts the phonon bottleneck, and the renormalized result, Eq. (25), where the energy δ conditions can be met by the spectral continuum of $\hat{G}(\omega)$.

Examples for the QD spectral functions are provided in Fig. 5, where the energy is given in units of the phonon energy $\hbar\omega_{\mathrm{LO}}$. The QD model assumes two confined states, s and p, for which in the left-hand column a separation by 1.1 $\hbar\omega_{\mathrm{LO}}$ has been chosen. The nominal ground state is 2.2 $\hbar\omega_{\mathrm{LO}}$ below the WL. The spectral functions show phonon satellites, representing higher-order processes due to multiphonon emission and absorption. The peaks are further broadened by Coulomb interaction between the carriers, even at the considered low WL-carrier density. In the left-hand column, the hybridization emerges since the phonon satellites of one shell are located in the vicinity of the other shell. The right-hand column corresponds to a situation in which the level spacing is considerably smaller than the phonon energy. Nevertheless, in both cases, a substantial overlap according to Eq. (26) is obtained, which facilitates efficient carrier scattering. The increased broadening of the peaks for higher temperatures is an important contribution to the experimentally observed temperature dependence of the transition rates. This effect is missing in the perturbative Boltzmann scattering rates.

IV. NUMERICAL RESULTS

A. QD model

In the subsequent calculations, we consider an ensemble of identical QDs which are randomly distributed with a density of 1×10^{10} cm^{-2}, containing a confined ground state and a first excited energy shell. Thus, we omit higher excited confined states, indicated by the experimental results, for numerical simplicity. Assuming a cylindrical symmetry and parabolic in-plane confinement, the excited shell is twofold degenerate. The energy-level spacing in the QD is chosen as 20 meV for

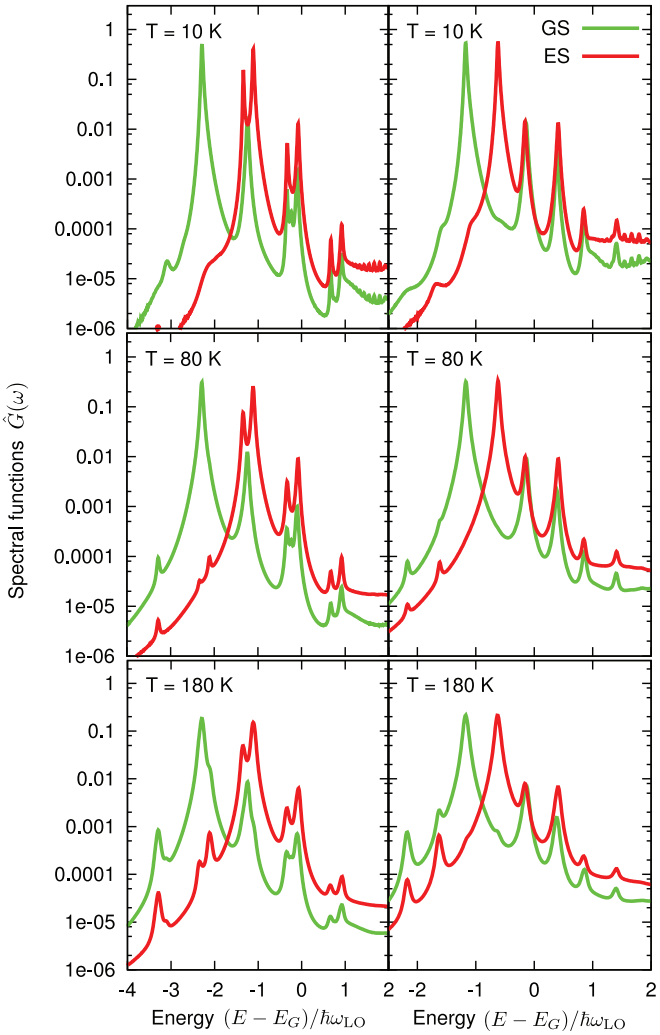

FIG. 5. (Color online) Spectral functions of the electronic ground state (GS) and excited state (ES) with the empty QD as reference state $|\Phi\rangle$ for different temperatures and a WL-carrier density of 3.2×10^9 cm^{-2}. For their calculation, both polaronic and carrier-carrier renormalizations are utilized. The left-hand (right-hand) column is for a QD-level spacing of 40 meV (20 meV) for electrons and 15 meV (8 meV) for holes. The energy is given relative to the WL band edge in units of the LO-phonon energy.

electrons and 8 meV for holes, with the same values for the distance of the excited shell below the continuum. The resulting interband energy differences correspond to the studied experimental situation. For the calculations, standard InGaAs material parameters for the effective masses, dielectric constants, and the LO-phonon energy of 36 meV have been used.

For the calculation of the Coulomb matrix elements, the QD states are described by a two-dimensional in-plane confinement and a finite-height potential confinement in the growth direction.[47] Orthogonalized plane waves are used for the WL states.[27,48]

When calculating the time evolution of the QD carrier population, we consider as the initial state empty QDs. For optical excitation of the delocalized states with short laser pulses, it is assumed that the carriers thermalize rapidly on a time scale that is faster than the considered time for the QD

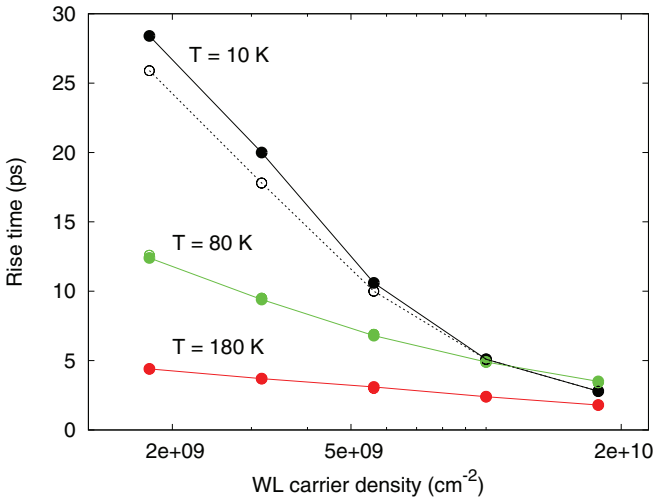

FIG. 6. (Color online) Rise time of the TRDT signal for the QD ground state calculated as a function of the WL carrier density for different temperatures. Both carrier-carrier and carrier-phonon interactions are considered within a nonperturbative theory including joint quasiparticle renormalizations. Results for the multiexciton configuration-picture description (solid circles) and single-particle description (open circles) are shown. For 80 and 180 K the corresponding results are practically identical.

carrier capture, thus leading to the discussed quasiequilibrium situation for the reservoir population.

B. Comparison with experimental results

Figure 6 collects the results for the rise times of the total electron plus hole ground-state occupancies, calculated for various temperatures and WL carrier densities in the presence of the interactions with both reservoirs. As a general trend we find a higher temperature sensitivity at lower WL carrier densities, which points to a dominant role of the phonon scattering in this regime. For low temperatures, the transition rate increases strongly with the WL carrier density due to more efficient carrier-carrier scattering (Auger-like processes assisted by WL carriers). The latter also causes stronger broadening of the spectral functions, which in turn accelerates carrier-phonon scattering as well. For elevated temperatures, the density dependence is weak due to a strong phonon contribution. These general trends as well as the quantitative results for the transition rates are in good agreement with the experiment; see Fig. 2. As we show below, renormalization effects are of critical importance for this agreement: Phonon and Coulomb scattering cannot be considered separate entities. Also a more detailed discussion of the temperature and carrier-density dependence of the scattering processes is given below.

A direct comparison between the many-particle configuration-picture description of QD excitations (solid symbols) and the single-particle description (open circles) in Fig. 6 shows a small difference for low temperatures and a negligible difference at elevated temperatures. This is due to the fact that the rise-time dynamics is mostly determined by carrier capture processes, which are slower than the subsequent relaxation processes of carriers within the QD. For the capture, the dominant processes are the

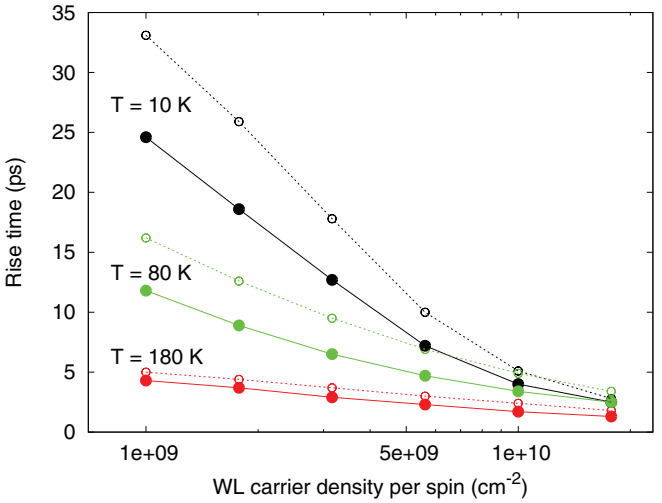

FIG. 7. (Color online) Same as Fig. 6 using the single-particle description. Results are compared for the inclusion of both spin subsystems (solid circles) and when considering only one spin subsystem, i.e., neglecting the influence of the other spin polarization (open circles).

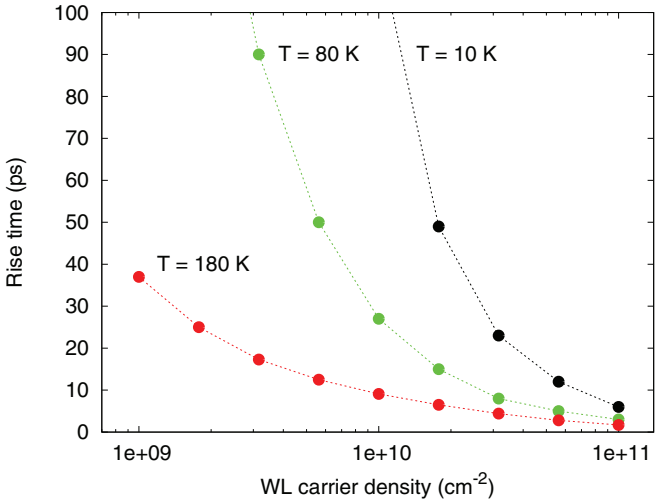

FIG. 8. (Color online) Same as Figs. 6 and 7 using the single-particle description and both spin subsystems. Instead of nonperturbative transition rates, now Boltzmann scattering integrals are used.

carrier transitions from the WL to a QD state, assisted either by LO phonons or another WL carrier moved to higher energies. Only one of the involved states belongs to the QD, while the other states represent quasicontinuous degrees of freedom. Then the approximate treatment of QD carrier correlations in the single-particle description (corresponding to a factorization approximation for carrier correlations) seems to be a reasonable approach for these processes when compared to the full treatment of QD carrier correlations within the von Neumann equation (which accounts for the transition of the QD between two many-body configurations). To simplify the numerical treatment of the latter, we have considered in Fig. 6 only one spin subsystem.

Since, in the present situation, the carrier dynamics is well represented within a single-particle description, we proceed on this level to extend the calculation to both spin subsystems. As can be seen in Fig. 7, except for low densities as well as low temperatures, the rise time increases only weakly when including the contributions of both spin subsystems. On a perturbative level, the carrier-phonon interaction would be unaffected. Within our nonperturbative description, the inclusion of both spins enters via quasiparticle renormalizations. As it turns out, this is the origin for the observed changes at low carrier densities in Fig. 7: Correlation contributions to the QD energy renormalizations reduce the energetic distance between the QD and WL states, thus increasing the efficiency of carrier-phonon interaction. This underscores the importance of considering Coulomb renormalizations for the states involved in carrier-phonon interaction processes. For the Coulomb processes, the other spin subsystem provides additional scattering partners, but also additional screening of the Coulomb interaction. The net result is a small increase in the Coulomb scattering rate at higher WL carrier densities.

As a last step, we use in the single-particle description transition rates calculated from Fermi's golden rule. In this case, the rates depend only on free-carrier energies, and energy renormalizations due to excited carriers (both in the QD and WL) are absent. This precludes not only energy shifts and polaron sidebands, but also the self-consistent level broadening associated with the scattering itself. The corresponding rise-time results in Fig. 8 exhibit a completely different behavior with a density and temperature dependence clearly deviating from the experimental results in Fig. 2.

As it turns out, the use of renormalized spectral functions for the calculation of transition rates substantially increases the number of scattering possibilities in comparison to the available scattering channels in terms of free-particle energies. Polaron renormalizations lead to additional phonon sidebands and the Coulomb interactions broaden these resonances. This also softens the resonance conditions for the processes involving monoenergetic LO phonons, as illustrated in Fig. 9(a). When considering only the interaction between WL and QD carriers via LO phonons within a nonperturbative treatment (using renormalized spectral functions), scattering is not restricted to the case where the energy difference of the electronic levels matches the LO-phonon energy. However, at the considered low temperature, the resonance condition is well pronounced (green symbols). When additionally including in the used spectral functions the broadening due to Coulomb interaction between QD and WL carriers, the LO-phonon resonance is less pronounced (blue circles). Including the Coulomb scattering itself (with fully renormalized spectral functions), even at the considered low carrier density, the phonon resonance is further weakened (red squares). Also the phonon resonance is much less pronounced at elevated carrier densities [Fig. 9(b)] and temperatures (not shown).

C. Density and temperature dependence of the population dynamics

So far we have only discussed the rise time of the ground-state population. The population dynamics itself provides additional information about the efficiency of scattering processes and its nontrivial interplay. As we show, the efficiency of carrier-phonon scattering increases faster with temperature

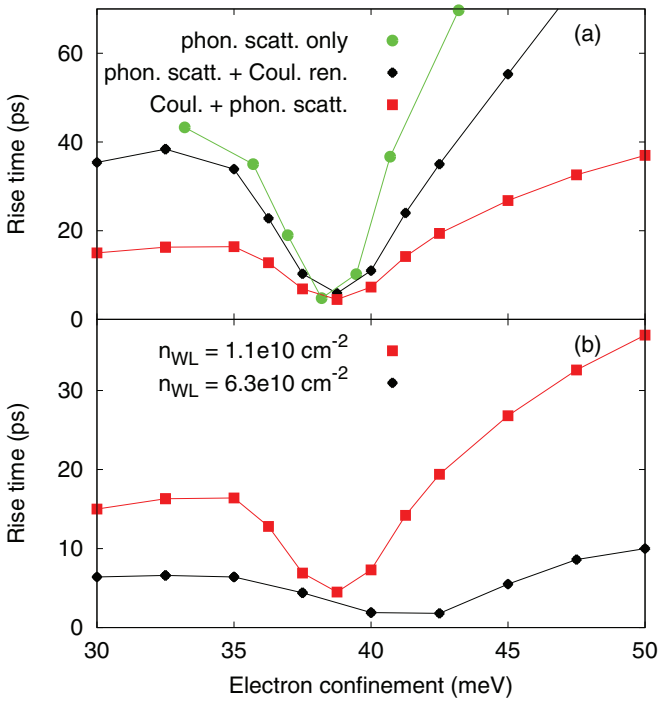

FIG. 9. (Color online) (a) Rise time of the TRDT signal for the QD ground state calculated as a function of the electron confinement energy for a WL carrier density $n_{\mathrm{WL}} = 1.1 \times 10^{10}$ cm^{-2} and 5 K. Results including both carrier-carrier and carrier-phonon interactions within a nonperturbative theory using joint quasiparticle renormalizations (red squares) are compared with nonperturbative scattering rates considering only the interaction with LO phonons but including in the spectral functions also Coulomb shifts and broadenings (black circles) and nonperturbative scattering rates only for LO phonons (green circles). In the latter case, instantaneous Coulomb energy shifts are included for better comparison. (b) Carrier-density dependence of the rise time based on the full calculation. For all curves, the single-particle description including both spin subsystems is used.

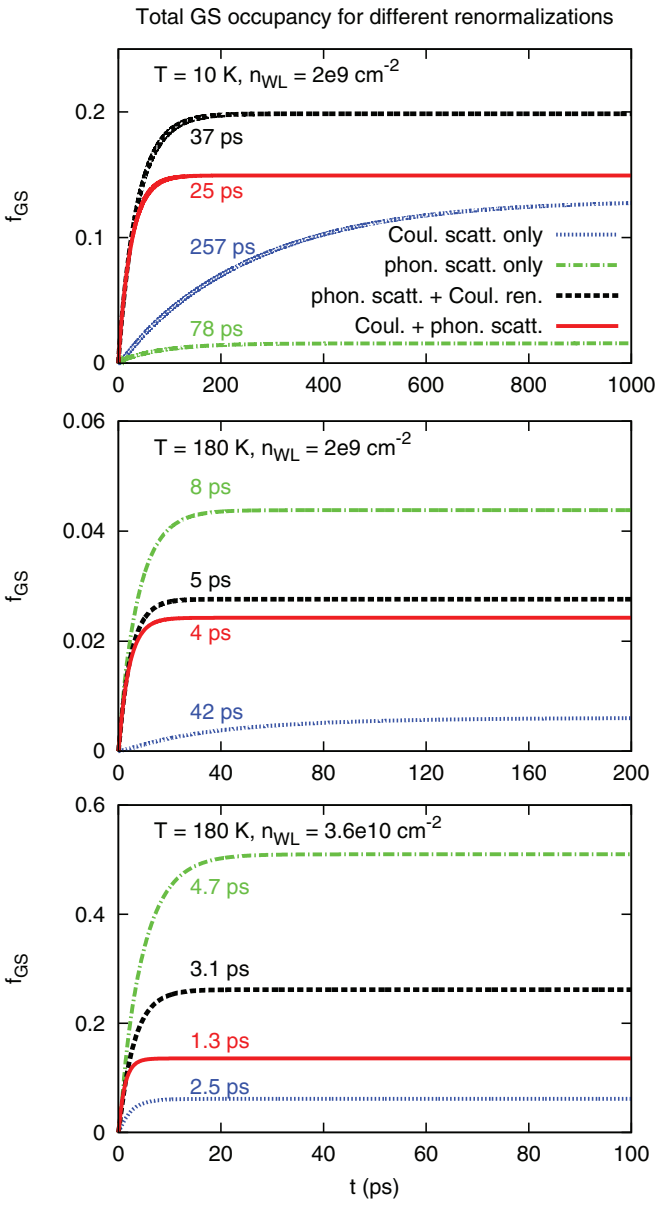

FIG. 10. (Color online) Time evolution of the sum of the QD electron and hole ground-state population for various carrier densities and temperatures. Results considering only nonperturbative carrier-phonon scattering (dash-dotted green line), nonperturbative carrier-phonon scattering with spectral functions containing polaron and Coulomb (Hartree-Fock and scattering) renormalizations (dashed black line), solely Coulomb scattering with accordingly renormalized spectral functions (dotted blue line), and the full result including mutual renormalizations (solid red line) are provided. In all cases, the single-particle description including both spin subsystems is used. Exponential fits for the rise time are given for each curve.

than the Coulomb scattering. Nevertheless, also the Coulomb scattering has its own temperature dependence, mainly via the population functions of the initial WL states, which are more spread out at elevated temperatures. In turn, the Coulomb scattering efficiency increases faster with carrier density than the carrier-phonon scattering. But the latter also has a clear carrier-density dependence via the population factors of the initial states for the scattering processes and via the carrier-density dependence of Coulomb renormalizations entering in the spectral functions.

This general trend and further details are provided in Fig. 10, where we compare the QD ground-state population dynamics due to the separate interaction with each reservoir (WL carriers, LO phonons) to those in which the reservoirs co-act self-consistently.

The top graph of Fig. 10 shows the time evolution of the sum of the QD electron and hole ground-state population for low temperature and WL carrier density. When considering carrier scattering due to LO phonons alone (in a nonperturbative theory using spectral functions only with LO-phonon renormalizations; green dash-dotted line), the rise time is much smaller than if carrier-carrier Coulomb scattering is used alone (in a nonperturbative theory using spectral functions only with Coulomb renormalizations; blue dotted line). On the other hand, the phonon scattering alone leads to a much smaller QD population. When both Coulomb and LO-phonon scattering co-act self-consistently, *the population increase is considerably faster than if one would add independent processes*. In the present case, the LO-phonon scattering gains a lot from the Coulomb broadening of the spectral functions.

This can be seen from the black dashed line, which represents the LO-phonon scattering contributions alone, calculated with spectral functions containing both polaron and Coulomb renormalizations. The latter case is rather close to the full result. Hence LO-phonon scattering is dominant in this regime, but only with the help of broadening effects in the spectral functions due to Coulomb scattering.

The middle graph addresses the same situation for increased temperature. Then the LO-phonon scattering alone becomes considerably more efficient. The Coulomb scattering alone is also faster albeit with reduced stationary population. Both effects are the result of the changes in the WL population, which provides additional capture processes as well as increased possibility for the reverse processes (QD carrier escape). The self-consistent rate considering both processes (red line) is again faster but the carrier escape lowers the stationary population.

This trend continues at elevated carrier densities (bottom graph). Clearly the Coulomb scattering benefits more strongly from the increasing WL carrier density, but the carrier-phonon scattering is also accelerated (different abscissas should be noted). In this case, both Coulomb and LO-phonon scattering contribute comparably to the full dynamics.

As a general observation from the shown results, we conclude that the interplay of carrier scattering due to Coulomb and LO-phonon interaction is not additive and has a nontrivial dependence on excitation conditions and QD level spacing. Coulomb interaction can further accelerate the carrier scattering due to LO-phonon interaction; it may, however, reduce the achievable QD population.

V. CONCLUSIONS

The QD carrier dynamics under the influence of Coulomb scattering and interaction with LO phonons was studied in an experiment-theory comparison. Fast population of the QD states after optical excitation into the barrier states is observed. The rise time of the QD population strongly changes with temperature for weak excitation and is temperature insensitive for strong excitation. In the used theoretical model, LO phonons and WL carriers play the role of reservoirs, which ensure irreversible dissipation and population redistribution of the QD carriers toward equilibrium. The results of two theoretical formalisms are compared: the von Neumann–Lindblad equation for the full QD density operator and kinetic equations for the single-particle occupation probabilities. For the considered carrier-capture processes from a quasicontinuum of delocalized states and the subsequent relaxation processes within the QDs, mediated by the reservoirs, both formalisms lead to identical results except for low temperatures and carrier densities. Agreement with the experimental results is only obtained when—in both cases—nonperturbative scattering rates are used. The latter account for polaron renormalization effects of the electronic states and additional broadening effects due to Coulomb scattering processes.

ACKNOWLEDGMENTS

The authors acknowledge financial support from the Deutsche Forschungsgemeinschaft (DFG) and the Bundesministerium für Bildung und Forschung (BMBF), as well as a grant for CPU time at the Norddeutscher Verbund für Hoch- und Höchstleistungsrechnen (HLRN).

[1] T. S. Sosnowski, T. B. Norris, H. Jiang, J. Singh, K. Kamath, and P. Bhattacharya, Phys. Rev. B **57**, R9423 (1998).
[2] J. Urayama, T. B. Norris, J. Singh, and P. Bhattacharya, Phys. Rev. Lett. **86**, 4930 (2001).
[3] F. Quochi, M. Dinu, N. H. Bonadeo, J. Shah, L. N. Pfeiffer, K. W. West, and P. M. Platzman, Physica B **314**, 263 (2002).
[4] F. Quochi, M. Dinu, L. N. Pfeiffer, K. W. West, C. Kerbage, R. S. Windeler, and B. J. Eggleton, Phys. Rev. B **67**, 235323 (2003).
[5] P. Borri, W. Langbein, U. Woggon, V. Stavarache, D. Reuter, and A. D. Wieck, Phys. Rev. B **71**, 115328 (2005).
[6] H. Kurtze, J. Seebeck, P. Gartner, D. R. Yakovlev, D. Reuter, A. D. Wieck, M. Bayer, and F. Jahnke, Phys. Rev. B **80**, 235319 (2009).
[7] A. Laucht, M. Kaniber, A. Mohtashami, N. Hauke, M. Bichler, and J. J. Finley, Phys. Rev. B **81**, 241302 (2010).
[8] U. Bockelmann and T. Egeler, Phys. Rev. B **46**, 15574 (1992).
[9] T. Inoshita and H. Sakaki, Phys. Rev. B **46**, 7260 (1992).
[10] I. Vurgaftman, Y. Lam, and J. Singh, Phys. Rev. B **50**, 14309 (1994).
[11] A. L. Efros, V. A. Kharchenko, and M. Rosen, Solid State Commun. **93**, 281 (1995).
[12] T. Inoshita and H. Sakaki, Phys. Rev. B **56**, 4355 (1997).
[13] A. V. Uskov, F. Adler, H. Schweizer, and M. H. Pilkuhn, J. Appl. Phys. **81**, 7895 (1997).
[14] M. Brasken, M. Lindberg, M. Sopanen, H. Lipsanen, and J. Tulkki, Phys. Rev. B **58**, 15993 (1998).
[15] H. Jiang and J. Singh, IEEE J. Quantum Electron. **34**, 1188 (1998).
[16] R. Ferreira and G. Bastard, Appl. Phys. Lett. **74**, 2818 (1999).
[17] T. Stauber, R. Zimmermann, and H. Castella, Phys. Rev. B **62**, 7336 (2000).
[18] K. Lüdge, M. J. P. Bormann, E. Malić, P. Hövel, M. Kuntz, D. Bimberg, A. Knorr, and E. Schöll, Phys. Rev. B **78**, 035316 (2008).
[19] K. Kral and Z. Khas, Phys. Rev. B **57**, 2061 (1998).
[20] O. Verzelen, R. Ferreira, G. Bastard, T. Inoshita, and H. Sakaki, Phys. Status Solidi B **190**, 213 (2002).
[21] J. Seebeck, T. R. Nielsen, P. Gartner, and F. Jahnke, Phys. Rev. B **71**, 125327 (2005).
[22] P. Gartner, J. Seebeck, and F. Jahnke, Phys. Rev. B **73**, 115307 (2006).
[23] H. Haug and A.-P. Jauho, *Quantum Kinetics in Transport and Optics of Semiconductors* (Springer, Berlin, 1996).
[24] W. Schäfer and M. Wegener, *Semiconductor Optics and Transport Phenomena* (Springer-Verlag, Berlin, 2002).
[25] A. V. Baranov, A. V. Fedorov, I. D. Rukhlenko, and Y. Masumoto, Phys. Rev. B **68**, 205318 (2003).
[26] A. V. Fedorov, A. V. Baranov, I. D. Rukhlenko, and S. V. Gaponenko, Phys. Rev. B **71**, 195310 (2005).
[27] T. R. Nielsen, P. Gartner, and F. Jahnke, Phys. Rev. B **69**, 235314 (2004).

[28]T. R. Nielsen, P. Gartner, M. Lorke, J. Seebeck, and F. Jahnke, Phys. Rev. B **72**, 235311 (2005).
[29]H. C. Schneider, W. W. Chow, and S. W. Koch, Phys. Rev. B **70**, 235308 (2004).
[30]M. Lorke, T. R. Nielsen, J. Seebeck, P. Gartner, and F. Jahnke, Phys. Rev. B **73**, 085324 (2006).
[31]K. Schuh, P. Gartner, and F. Jahnke, Phys. Rev. B **87**, 035301 (2013).
[32]A. Steinhoff, P. Gartner, M. Florian, and F. Jahnke, Phys. Rev. B **85**, 205144 (2012).
[33]G. Ortner, M. Schwab, M. Bayer, R. Pässler, S. Fafard, Z. Wasilewski, P. Hawrylak, and A. Forchel, Phys. Rev. B **72**, 085328 (2005).
[34]M. Schwab, H. Kurtze, T. Auer, T. Berstermann, M. Bayer, J. Wiersig, N. Baer, C. Gies, F. Jahnke, J. P. Reithmaier *et al.*, Phys. Rev. B **74**, 045323 (2006).
[35]T. Berstermann, T. Auer, H. Kurtze, M. Schwab, D. R. Yakovlev, M. Bayer, J. Wiersig, C. Gies, F. Jahnke, D. Reuter *et al.*, Phys. Rev. B **76**, 165318 (2007).
[36]H. Kurtze, D. R. Yakovlev, D. Reuter, A. D. Wieck, and M. Bayer, Phys. Rev. B **85**, 195303 (2012).
[37]S. Raymond, S. Studenikin, A. Sachrajda, Z. Wasilewski, S. J. Cheng, W. Sheng, P. Hawrylak, A. Babinski, M. Potemski, G. Ortner *et al.*, Phys. Rev. Lett. **92**, 187402 (2004).
[38]M. Grundmann and D. Bimberg, Phys. Rev. B **55**, 9740 (1997).
[39]M. Grundmann and D. Bimberg, Phys. Status Solidi A **164**, 297 (1997).
[40]P. Borri, V. Cesari, and W. Langbein, Phys. Rev. B **82**, 115326 (2010).
[41]N. Baer, P. Gartner, and F. Jahnke, Eur. Phys. J. B **42**, 231 (2004).
[42]H. J. Carmichael, *Statistical Methods in Quantum Optics 1: Master Equations and Fokker-Planck Equations (Theoretical and Mathematical Physics)* (Springer, New York, 2003).
[43]G. D. Mahan, *Many-Particle Physics* (Plenum Press, New York, 1993).
[44]U. Bockelmann and G. Bastard, Phys. Rev. B **42**, 8947 (1990).
[45]H. Benisty, C. M. Sotomayor-Torres, and C. Weisbuch, Phys. Rev. B **44**, 10945 (1991).
[46]P. Danielewicz, Ann. Phys. **152**, 239 (1984).
[47]A. Wojs, P. Hawrylak, S. Fafard, and L. Jacak, Phys. Rev. B **54**, 5604 (1996).
[48]H. C. Schneider, W. W. Chow, and S. W. Koch, Phys. Rev. B **64**, 115315 (2001).